SUPPLEMENTARY INFORMATION

RESULTS

The binding of the Ser-AMP analog to the anticodon-binding domain of MST1 resembles the interaction between MST1 and the anticodon loop—Unexpectedly, the MST1-SAM crystal contained an additional SAM molecule bound to the anticodon-binding domain of MST1 (Figs. 4*A* and S4). The nature of interactions and the extent of the conformational change in the anticodon-binding domain promoted by the analog binding suggest that the interaction is reminiscent of the mechanism by which MST1 recognizes the anticodon sequence in $tRNA_2^{Thr}$.

The Ser-AMP analog interacts with the site implicated in recognition of the anticodon loop of threonine tRNA. An experimental electron density map calculated to 2.87 Å resolution with the Fo-Fc amplitude differences as coefficients and the phase that was obtained by molecular replacement with the apo MST1 as a search model, revealed a strong positive peak near the anticodon-binding domain (Fig. S2*B*). The shape of the continuous positive electron density clearly suggests the presence of an adenosine modified at its O5' hydroxyl. Because only SAM was used in the soaking experiments, the density was interpreted and modeled as the non-hydrolyzable analog of the Ser-AMP conjugate. The Fo-Fc difference map also indicates that strands β19, loop β18-β19 and helix α11 undergo a conformational change upon binding the analog (Fig. S4*A*). These structural elements move towards one another thus forming a pocket for SAM. Moreover, a series of side chains in this region either adopt different orientations or are more structured upon SAM binding (Fig. S4*B*). In particular, the side chain of Arg439 from loop β18-β19 is disordered in both the apo MST1 and MST1-TAM structures, but it is completely ordered in the MST1-SAM crystal. Along with Ile411 from helix α11, Arg439 stacks the adenine ring and orients the Hoogsteen face towards the side chain of Arg434 in strand β18 (Fig. S4*C*). The orientation of Arg434 is, in turn, stabilized by van der Waals interactions with Phe442 from loop β18-β19 (Fig. S4*B*). A comparison with apo MST1 reveals that the side chains of Arg434 and Phe442 rotate in concert around the Cβ-Cγ and Cα-Cβ bonds, respectively, on SAM binding. Interactions with Arg434, Arg439 and Ile411 are the only specific interactions between the anticodon-binding domain of MST1 and SAM. The rest of the Ser-AMP analog does not directly interact with MST1, but is rather surrounded with solvent molecules coordinated with the side chains of Glu425 and Asn432 (data not shown).

The interaction between the analog and the anticodon-binding domain is likely due to a high concentration of the analog used in the soaking experiments and therefore could be viewed as an artifact or a fortuitous event. We hypothesized that the nature of interactions between SAM and the anticodon-binding domain could resemble the interactions between the enzyme and the anticodon loop of $tRNA^{Thr}$. Indeed, when the Cα atoms of the *E. coli* ThrRS bound to $tRNA^{Thr}$ (PDBID: 1QF6) were superimposed onto the corresponding atoms in MST1 complexed with SAM (r.m.s.d. value of 1.37 Å), and after applying the resulting transformation matrix onto the *E. coli* $tRNA^{Thr}$, it became evident that the adenine of a nucleotide in position 37 in the anticodon loop of $tRNA^{Thr}$ almost perfectly superimposed onto the adenine in SAM (Fig. S5). Furthermore, the sugar-phosphate backbone linking nucleotides 36 and 37 superimposed over the aminoacyl and sulfamoyl moieties in the Ser-AMP mimic (Fig. S5). These findings suggest that SAM binds a site on MST1 responsible for recognizing the 3'-end of the anticodon sequence in $tRNA^{Thr}$, and that its binding presumably induces a conformational change in the anticodon-binding domain similar to that of the cognate tRNA.

DISCUSSION

Implications for anticodon sequence recognition—MST1 binds and acts on two $tRNA^{Thr}$ species, one of which carries an enlarged anticodon loop with the CUN anticodon. While the

binding of the Ser-AMP mimic to the anticodon-binding domain does not play a role in pre-transfer editing of the reaction product, it does provide the first glimpse into the mechanism of the anticodon-loop binding by MST1. Even though the adenine ring of SAM almost perfectly superimposes with A37 in the anticodon loop of *E. coli* $tRNA^{Thr}$ (Fig. S5), we cannot suggest that Arg434 recognizes specifically A37 in $tRNA^{Thr}$. In fact, we have previously shown that Arg434 does not play a role in binding $tRNA_2^{Thr}$, which is the only mitochondrial $tRNA^{Thr}$ that contains A37. Moreover, because A37 is modified *in vivo*, the interaction between its Hoogsteen face and Arg434 would not be plausible. However, the binding of SAM to the anticodon-binding site does suggest that Arg434 is capable of interacting with an unmodified base in the anticodon loop. It is likely that this side chain is involved in specific recognition of the anticodon loop of an unusual $tRNA_1^{Thr}$. To understand the mechanism(s) at the structural level by which MST1 recognizes distinct anticodon loops, crystal structures of the MST1-$tRNA^{Thr}$ binary complexes are necessary.

FIGURE LEGENDS

Fig. S1. Spontaneous hydrolysis of Thr-AMP and Ser-AMP in solution. Thr-AMP and Ser-AMP were chased out of the active site of WT MST1 by addition of 20 mM cold ATP, and their spontaneous hydrolysis in solution was measured over time.

Fig. S2. SAM binds to both the aminoacylation and anticodon-binding sites in MST1. Electron-density map (green mesh) calculated with the Fo-Fc amplitude differences as coefficients and the phase obtained from molecular replacement with the apo MST1 (PDBID: 3UGQ) as a search model, shows unambiguously that SAM (blue balls-and-sticks) binds to both the aminoacylation pocket **(A)** and the anticodon-binding site of MST1 **(B)**. The difference map was calculated to 3-Å resolution and contoured at 3σ. Helices are dark red, strands are grey, loops are gold and the Zn^{2+} ion (in the active site) is an orange sphere.

Fig. S3. Sequence alignments of MST1 and *E. coli* ThrRS. The residues shown in Fig. 5 are highlighted with asterisks. *Sc*, *Saccharomyces cerevisiae*; *Kt*, *Kluyveromyces thermotolerans*; *Vp*, *Vanderwaltozyma polyspora*; *Cg*, *Candida glabrata*; *Ca*, *Candida albicans*; *Sp*, *Schizosaccharomyces pombe*; *Ec*, *Escherichia coli*.

Fig. S4. A conformational change in the anticodon-binding domain of MST1 induced by binding of the second SAM molecule. (A) Superimpositioning of apo-MST1 (beige) onto MST1-SAM (dark red) reveals that binding of SAM 2 (blue sticks) induces a conformational change in helix α11, loop β18-β19 and strand β19 in the anticodon-binding domain. These structural elements move towards one another thus enclosing the analog. **(B)** Side chains of Arg434 (strand β18) and Phe442 (loop β18-β19) swing ~180°, and the side chain of Arg439 is fully ordered on SAM 2 binding. **(C)** Arg439 and Ile411 (helix α11) stack the adenine ring and orient its Hoogsteen face for H-bond interactions with Arg434 (dashed lines).

Fig. S5. The interaction between SAM and the anticodon-binding domain of MST1 resembles that of the anticodon loop and ThrRS. Superimpositioning of the crystal structure of the *E. coli* ThrRS-$tRNA^{Thr}$ complex (light and dark green, respectively; PDBID: 1QF6) onto that of MST1-SAM (dark red) reveals that SAM 2 (blue balls-and-sticks) binds the same site in the anticodon-binding domain as A37 (green balls-and-sticks) of $tRNA^{Thr}$. The adenine rings of SAM 2 and A37 that are bound to the corresponding enzymes are almost perfectly superimposed. Additionally, the sulfamoyl and seryl groups in SAM mimic the sugar-phosphate backbone of $tRNA^{Thr}$.

Table S1. Hydrolysis of [γ-^{32}P] ATP by MST1 variants in the presence of 20 mM amino acids with or without $tRNA^{Thr}$

k (min^{-1})	Thr	Ser	Val	Ala	Cys	Thr + tRNA	Ser + tRNA
WT	2.4 ± 0.6	6.2 ± 1.0	0	0	0	2.7 ± 0.1	7.4 ± 0.3
R434A	3.0 ± 0.2	7.2 ± 0.1	ND	ND	ND	ND	ND

ND, not determined.

Table S2. Data collection and refinement statistics

Crystal	**MST1-SAM**
Space group	C 2_1
Unit cell dimensions	*a*= 213, *b*= 107, *c*=153 Å β=130.05°
Data collection	
Resolution limit (Å)	2.87
Unique reflections	60,275
Completeness (overall / last shell; %)	99 / 98
R_{sym} (overall / last shell; %)	13.7 / 73.2
I/σI (overall / last shell)	15 / 2.2
Redundancy (overall / last shell)	5.6 / 4.9
Refinement	
Average B-factor (Å^2)	
Protein	53.0
Ions, ligands and solvent	39.5
Number of atoms (protein)	13,613
Number of atoms (ions, ligand)	160
Number of solvent molecules	341
R_{work} (|F| > 0σ; %)	17.5
R_{free} (|F| > 0σ; %)	22.9
R.m.s. deviations from ideality:	
Bond lengths (Å)	0.003
Bond angles (°)	0.750

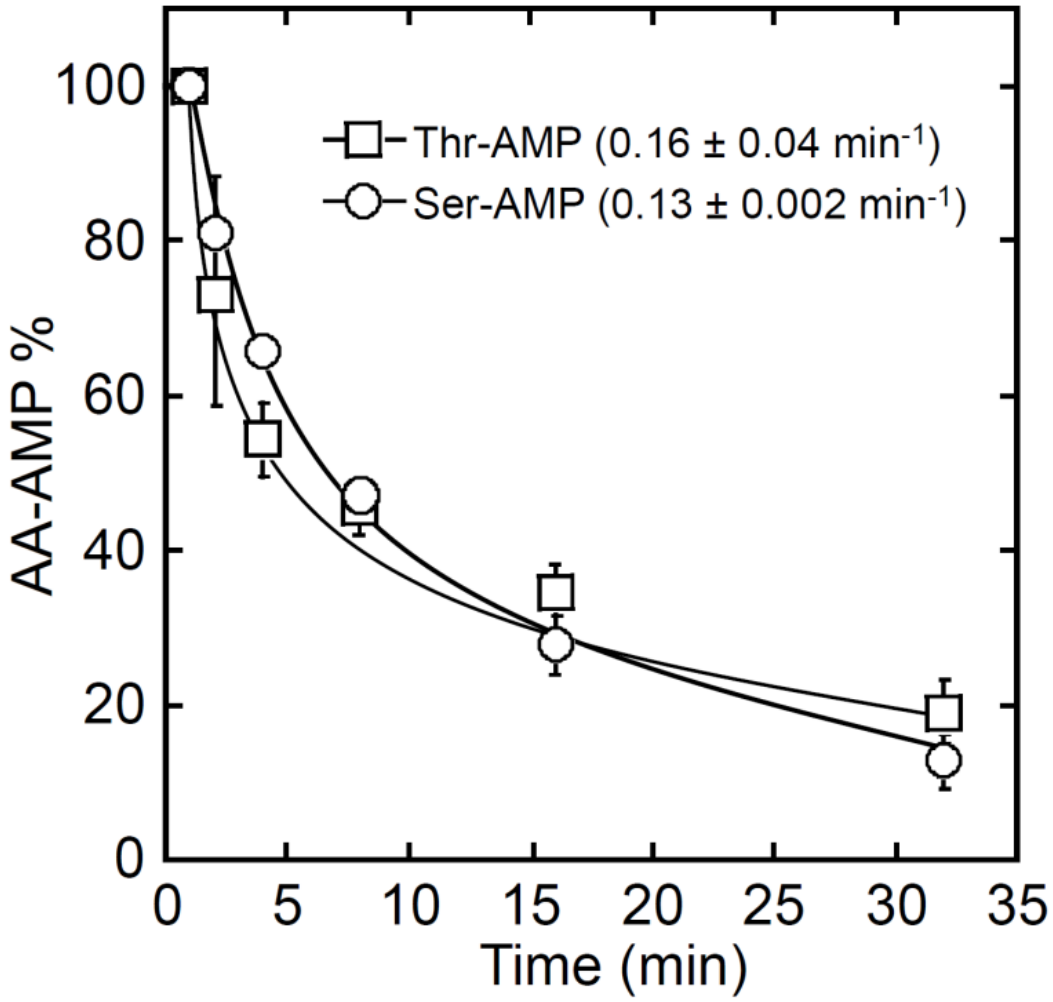

Ling *et al.* Figure S1

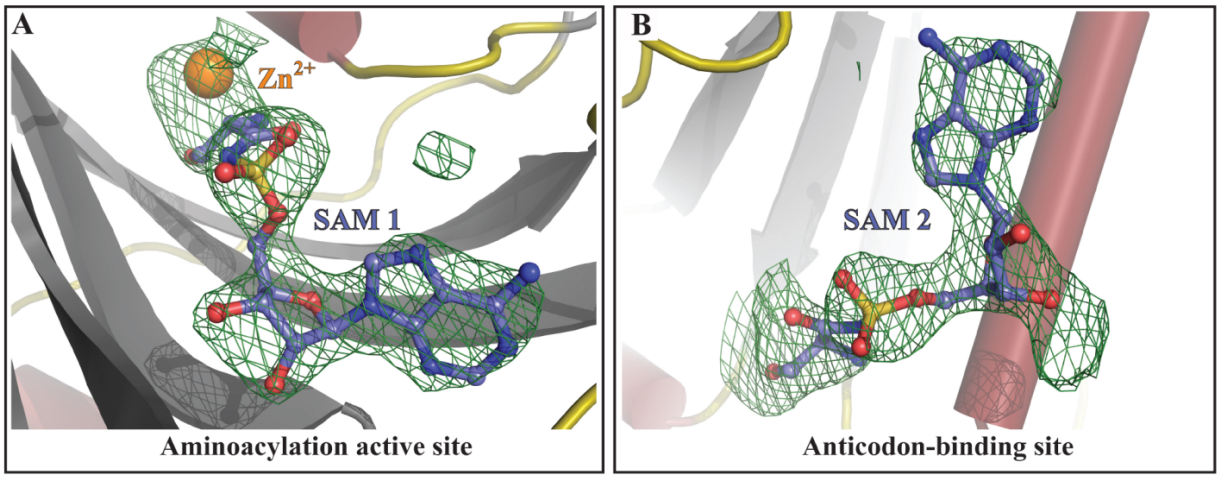

Ling *et al.* Figure S2

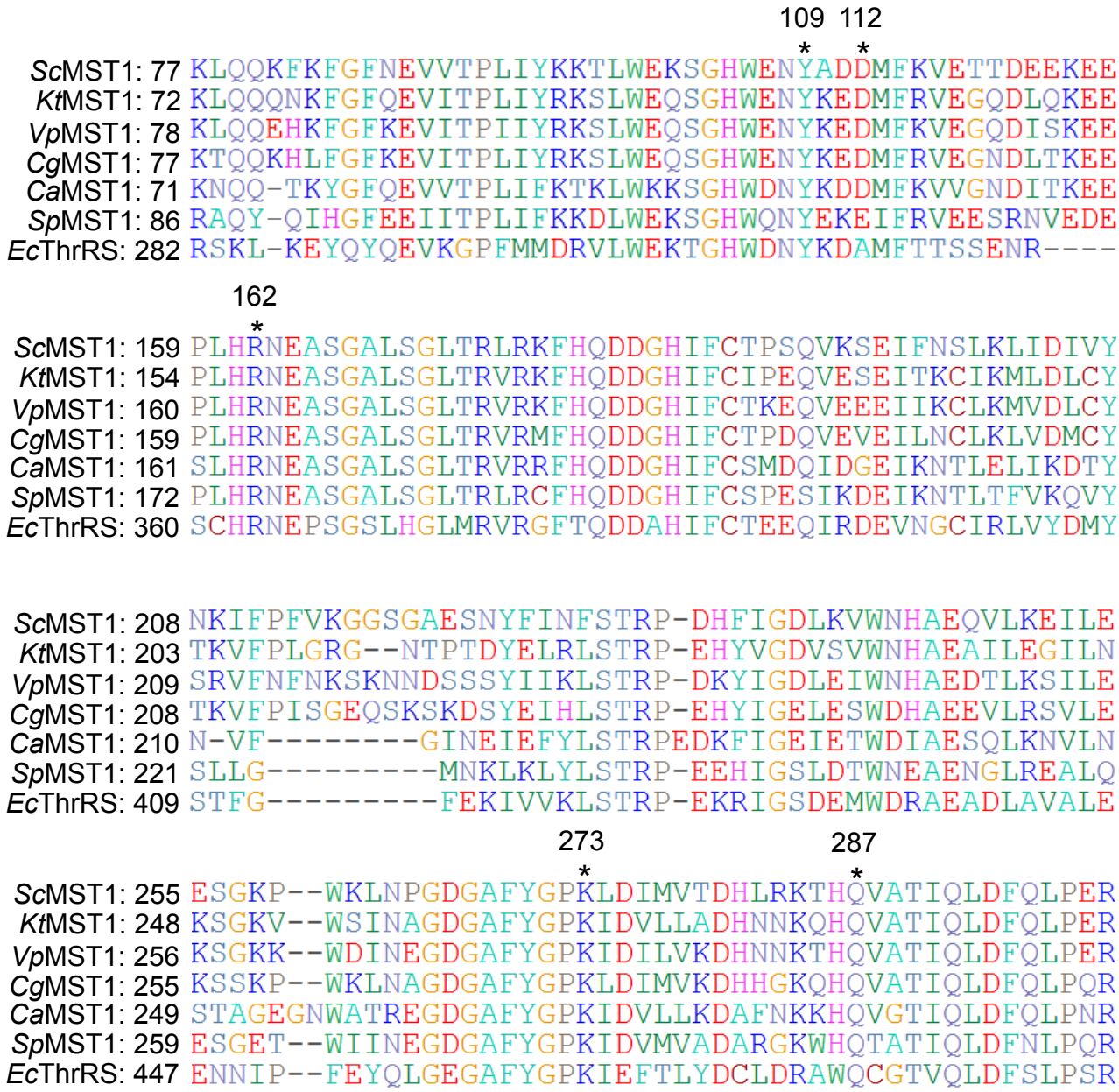

Ling *et al.* Figure S3

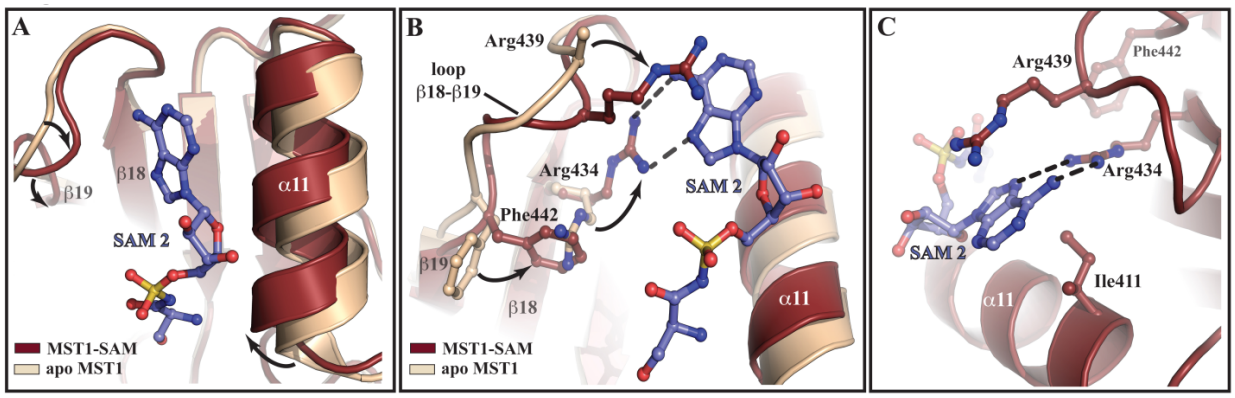

Ling *et al.* Figure S4

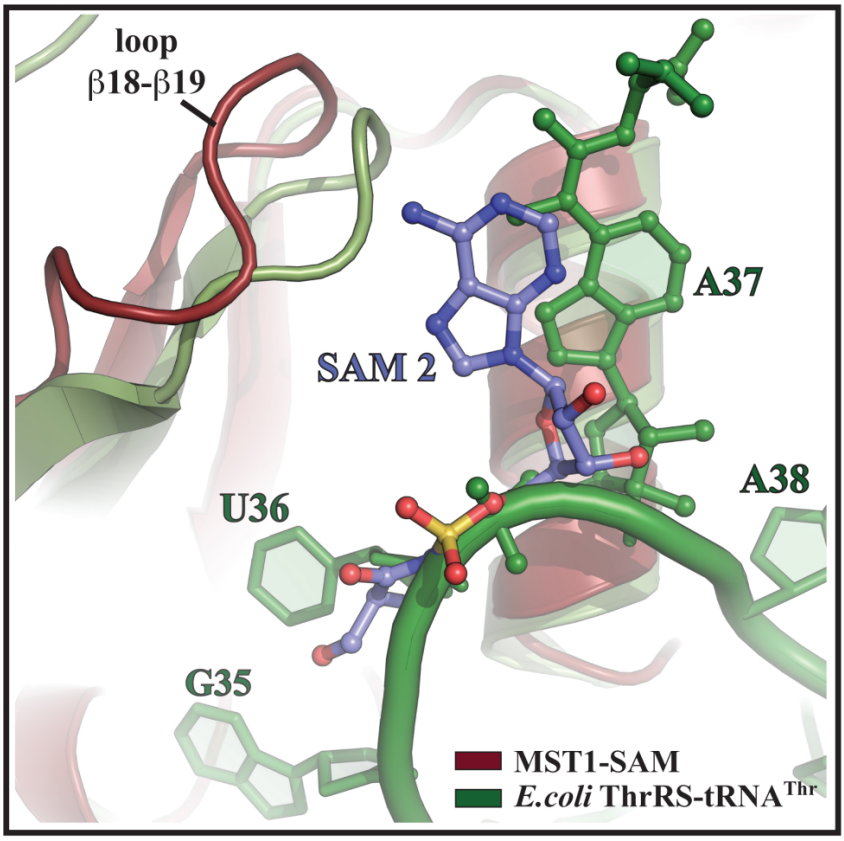

Ling *et al.* Figure S5